Nanoscale

PAPER

View Article Online
View Journal | View Issue

Cite this: *Nanoscale*, 2015, **7**, 6238

Antifungal nanofibers made by controlled release of sea animal derived peptide†

Juliane F. C. Viana,[a,b] Jéssica Carrijo,[b] Camila G. Freitas,[b,c] Arghya Paul,[d] Jarib Alcaraz,[e] Cristiano C. Lacorte,[f] Ludovico Migliolo,[b] César A. Andrade,[e] Rosana Falcão,[f] Nuno C. Santos,[g] Sónia Gonçalves,[g] Anselmo J. Otero-González,[h] Ali Khademhosseini,[d] Simoni C. Dias[b] and Octávio L. Franco*[a,b,i]

Received 2nd February 2015,
Accepted 25th February 2015

DOI: 10.1039/c5nr00767d

www.rsc.org/nanoscale

Candida albicans is a common human-pathogenic fungal species with the ability to cause several diseases including surface infections. Despite the clear difficulties of *Candida* control, antimicrobial peptides (AMPs) have emerged as an alternative strategy for fungal control. In this report, different concentrations of antifungal Cm-p1 (*Cencritchis muricatus* peptide 1) were electrospun into nanofibers for drug delivery. The nanofibers were characterized by mass spectrometry confirming the presence of the peptide on the scaffold. Atomic force microscopy and scanning electronic microscopy were used to measure the diameters, showing that Cm-p1 affects fiber morphology as well as the diameter and scaffold thickness. The Cm-p1 release behavior from the nanofibers demonstrated peptide release from 30 min to three days, leading to effective yeast control in the first 24 hours. Moreover, the biocompatibility of the fibers were evaluated through a MTS assay as well as ROS production by using a HUVEC model, showing that the fibers do not affect cell viability and only nanofibers containing 10% Cm-p1–PVA improved ROS generation. In addition, the secretion of pro-inflammatory cytokines IL-6 and TNF-α by the HUVECs was also slightly modified by the 10% Cm-p1–PVA nanofibers. In conclusion, the electrospinning technique applied here allowed for the manufacture of biodegradable biomimetic nanofibrous extracellular membranes with the ability to control fungal infection.

Introduction

Candida spp. are known to cause opportunistic infections in immunocompromised patients.[1,2] *Candida albicans* is considered the most common human-pathogenic fungal species, causing several diseases including life-threatening bloodstream and painful superficial infections.[3,4] Moreover, invasive candidiasis has been considered a significant cause of late-onset infection in premature infants.[5] Candidiasis is also known as the major cause of mortality and morbidity in immunocompromised patients as a result of AIDS, cancer chemotherapies or organ transplantation.[4,6] Despite the advances in treatment and management of fungal infections, there are several reports about resistant fungal strains, treatment failure and the scarcity of antifungal agents with low toxicity for systemic *C. albicans* infections.[6]

Despite the clear difficulties of *Candida* control, antimicrobial peptides (AMPs) have emerged as alternative compounds for pathogen control. These proteinaceous compounds show a wide spectrum of activities against pathogenic bacteria, fungi, viruses, parasites, as well as analgesic and immunomodulatory activities.[7–9] Cm-p1 (SRSELIVHQR) is an AMP isolated from *Cenchritis muricatus*, a snail-like Caribbean sea mollusk,[10] with bactericidal activity against *Staphylococcus aureus* and *Escherichia coli*. In complementary studies, Cm-p1 was chemically synthesized, functionally characterized and further evaluated regarding its antimicrobial activities, showing deleterious

[a]*Programa de Pós-Graduação em Patologia Molecular, Universidade de Brasília, Brazil. E-mail: ocfranco@gmail.com*
[b]*Programa de Pós-Graduação em Ciências Genômicas e Biotecnologia, Centro de Análises Proteômicas e Bioquímicas, Universidade Católica de Brasília, Brazil*
[c]*Instituto Federal de Educação, Ciência e Tecnologia de Brasília, Brasília, Brazil*
[d]*Biomaterials Innovation Research Center, Division of Biomedical Engineering, Brigham and Women's Hospital, Harvard Medical School/Wyss Institute for Biologically Inspired Engineering/Harvard-MIT Division of Health Sciences and Technology, Massachusetts Institute of Technology, Cambridge, USA*
[e]*Programa de Pós-Graduação em Ciências dos Materiais, Universidade Federal de Pernambuco, Recife, Brazil*
[f]*EMBRAPA Recursos Genéticos e Biotecnologia, Parque Estação Biológica, Brasília, Brazil*
[g]*Instituto de Medicina Molecular, Faculdade de Medicina, Universidade de Lisboa, Lisbon, Portugal*
[h]*Centro de Estudios de Proteínas, Facultad de Biología, Universidad de La Habana, Cuba*
[i]*S-Inova Pós-Graduação Biotecnologia, Universidade Católica Dom Bosco, Campo Grande, MS, Brazil*

†Electronic supplementary information (ESI) available. See DOI: 10.1039/c5nr00767d

activities against yeasts and filamentous fungi. Moreover, no toxicity against human red blood and RAW 264.7 cells was noted.[11]

For AMPs to function properly, they must be delivered at an appropriate dosage and time, which remains a significant challenge. Several works report self-assembling peptides in nanofibers for tissue engineering,[12] drug release[13] and biomaterial[14] production. Moreover, the use of electrospun nanofibers has been investigated for potential wound dressings, since the fibrous structure can protect wounds from microbial contamination, making it possible to incorporate antimicrobial agents, growth factors and antiseptics.[15,16] Antibiotics incorporated in electrospun nanofibers include silver compounds,[17–20] vancomycin,[21,22] gentamicin[21–23] and rifampicin.[24] However, some AMPs have also been employed in electrospun nanofiber mats.[13,25–30] Electrospinning is a promising tool for peptide nanofiber production.[31] This process allows nanofiber fabrication of diverse materials with diameters ranging from nanometers to micrometers, with high porosity, a large surface area[17,32] and efficient controlled drug release.[31] Here, the electrospinning feasibility for a synthetic antimicrobial peptide, Cm-p1, in nanofibers of poly(vinyl alcohol) (PVA) was explored in order to generate an antifungal wound dressing with protective activity against *Candida*. Furthermore, immunomodulatory activities, cellular viability and reactive oxygen species generation with different scaffold formulations were also determined. The scaffolds were further characterized by scanning electron and atomic force microscopies as well as by MALDI-TOF technology.

Results and discussion

Electrospun fiber mats of Cm-p1–PVA and peptide detection

Cm-p1–PVA-loaded nanofibrous membranes were fabricated by electrospinning PVA. During the electrospinning process, parameters such as voltage and distance between the needle and the collector were kept the same for every PVA and Cm-p1–PVA fiber. Earlier, Cm-p1 was solubilized in deionized water under stirring (200 rpm) and then 10% PVA was added to the peptide solution. The hydrophilic nature of Cm-p1 allowed its solubilization in deionized water. PVA, a synthetic polymer, has been widely used to produce electrospun fiber mats[33] attracting attention due to its biocompatibility, hydrophilicity, physical properties and chemical resistance.[34,35] Furthermore, PVA nanofibers have been applied in different fields, such as enzyme immobilization, electrode materials, sensors and biomedical applications.[36,37]

Firstly, MALDI TOF analyses of fibers were performed in order to identify the existence or absence of Cm-P1. Fig. 1a demonstrates the free Cm-p1 molecular mass (1224.48 Da). Moreover, an identical molecular mass was obtained by directly ionizing the nanofiber containing Cm-p1–PVA (Fig. 1b). The resulting observations reinforce the idea that the peptide is encapsulated within the fiber through weak inter-

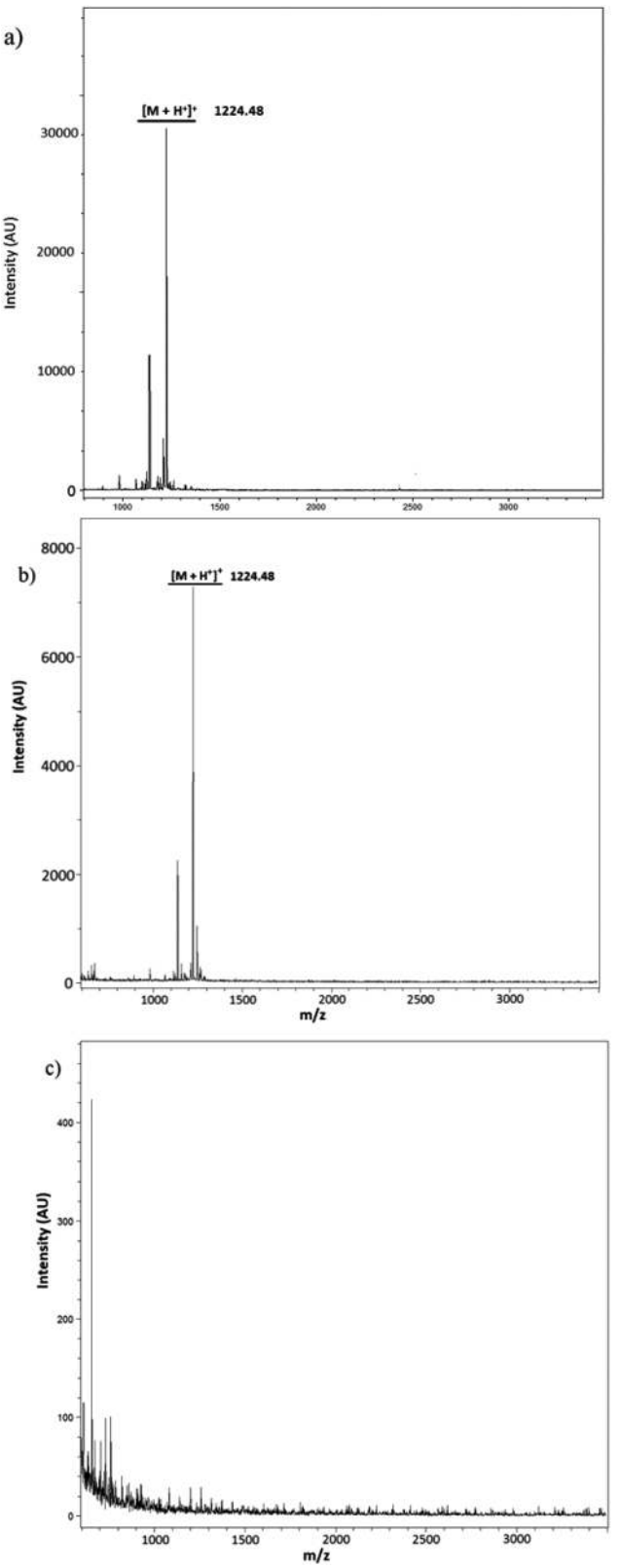

Fig. 1 MALDI TOF analysis of (a) free Cm-p1, (b) Cm-p1–PVA incorporated in an electrospun nanofiber and (c) the PVA nanofiber with no peptide.

actions. The PVA fiber, free of peptide, was also checked and demonstrated the complete absence of Cm-p1 (Fig. 1c).

Microscopic characterization of fibers

To better evaluate the resulting fibers, SEM was performed (Fig. 2a and b). The SEM micrographs in other magnifications can be seen in Fig. 1 in the ESI.† The average diameters of the spun fibers containing Cm-p1–PVA were 295.3 ± 44.9 nm, 293.5 ± 45.8 nm, 210.6 ± 47.1 nm for concentrations of 2.5% Cm-p1-PVA, 5% Cm-p1–PVA and 10% Cm-p1-PVA, respectively. Otherwise, for the PVA fibers without Cm-p1, the average diameter was 335.9 ± 28.2 nm. The nanofiber image characterizations in Fig. 2a and b show that the fiber diameters decrease with the presence of Cm-p1 when compared with the PVA fiber mat. Furthermore, the standard deviation observed in the control fibers was less than that in the fibers containing the peptide, indicating that the PVA control fibers are more homogeneous and bead-free in comparison to the fibers containing Cm-p1.

AFM was also used for further sample characterization since this technique can be used to measure soft and fragile adhesive surfaces, without harming the samples.[38] Indeed, the AFM images (Fig. 2c and d) confirmed the SEM results, showing that the thickness of the nanofibers containing 10% Cm-p1–PVA (1386 nm, Fig. 2b) was smaller than the PVA (1535 nm, Fig. 2a) spun fibers. In complementary measurements, the fiber diameters were also evaluated by AFM (Fig. 2c and d). As in the SEM measurements, the 2.5% Cm-p1–PVA (570.8 ± 81.6 nm) and 10% Cm-p1–PVA (550.2 ± 144.4 nm) samples presented smaller diameters than the control samples (990.9 ± 128.9 nm). However, by AFM, the diameter measurements were higher than with SEM in every sample analyzed. It is possible that during the SEM measurements the samples were dehydrated, decreasing the diameters of the fibers, and/or the diameters obtained by AFM are increased due to convolution with the tip diameter. The differences between PVA and Cm-p1–PVA fiber measurements were found to be significant (** $P < 0.0001$) both in the SEM and AFM measurements. Furthermore, the nanofibers were not uniform in the case of the 10% Cm-p1–PVA sample, according to Fig. 2a and b. This suggests that high concentrations of Cm-p1 may interfere with the fiber morphology, due to the insufficient stretching of the polymer jet during the electrospinning process through jet suspension and needle obstruction, leading to bead formation in the 10% Cm-p1–PVA mats. Nanofibers containing the antimicrobial peptide nisin also displayed a smaller diameter when compared with control fibers.[27]

Peptide nanofiber release

The peptide release from the Cm-p1–PVA nanofiber mats with different Cm-p1 content is shown in Fig. 3. The behavior of these nanofibers demonstrated peptide release from 30 min to three days, leading to effective yeast control in the first 24 h. Cm-p1 was rapidly released from the Cm-p1–PVA-loaded electrospun nanofiber mats. Fig. 3a shows that after 120 min, Cm-p1 was released into the dissolution medium from 2.5, 5 and

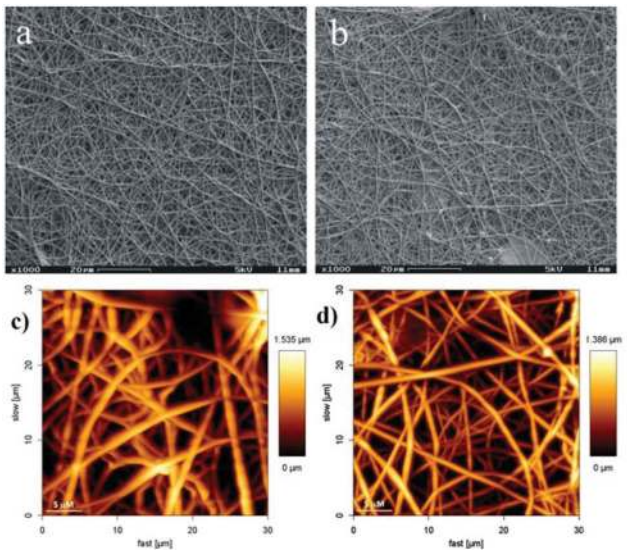

Fig. 2 SEM micrographs (a, b) and AFM images (c, d) of PVA and Cm-p1–PVA fibers. (a) 10% PVA fibers with 1000× magnification, (b) 10% Cm-p1–PVA fibers with 1000× magnification, (c) 10% PVA fibers and (d) 10% Cm-p1–PVA fibers.

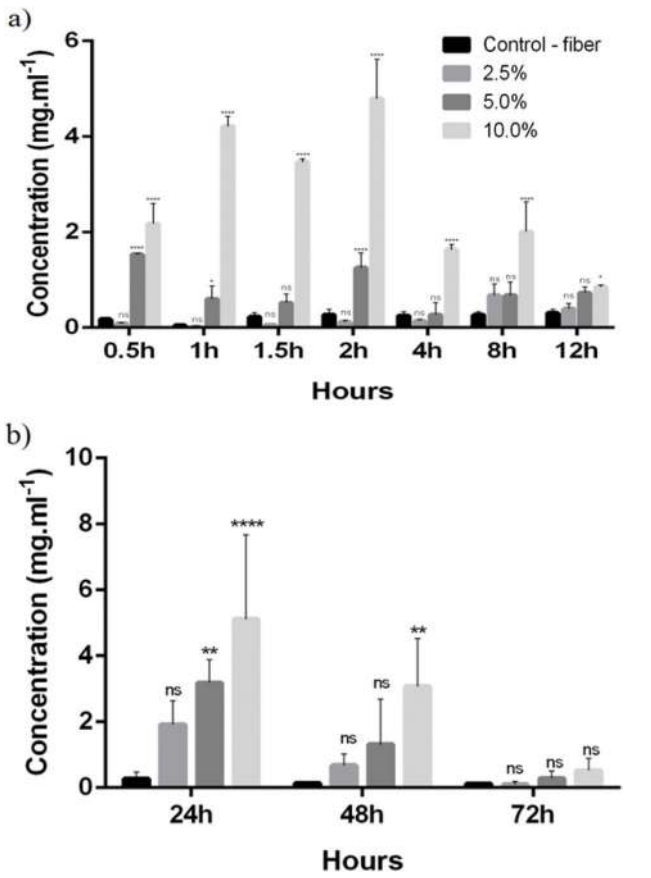

Fig. 3 Cm-p1–PVA release analyses from nanofibrous membranes (a) using different scaffolds over 12 h and (b) from the same scaffolds for 72 h. NS: no significance. (*$P < 0.1$; **$P < 0.01$; ****$P < 0.0001$).

10% Cm-p1–PVA nanofiber mats (Fig. 3a). In parallel, for cumulative peptide release, another nanofiber fragment was incubated in a glass tube at 37 °C. The buffer was changed every 24 h until 3 days without removal, and the Cm-p1 amount was quantified. Fig. 3b shows that the release of the Cm-p1–PVA spun fibers was higher during the first 24 h, gradually decreasing after 48 and 72 h, probably due to a reduction in the peptide concentration inside the fiber mat. Fig. 2 in the ESI† presents the Cm-p1 quantification by using HPLC chromatograms after 24 h of release; the quantified nanofiber release at every time evaluated with the triplicate media and standard deviation is shown in ESI Table 1.† Every sample was quantified by HPLC and the chromatograms do not show any alteration and modification in the spectrum, suggesting that during the release assay the peptide was stable. These values were also used to calculate the peptide quantity for the antifungal assays. It is of interest that Cm-p1 release was sustained after 48 h, which could be a desirable property for anti-infective biomaterials. The PVA nanofibers could provide a fast-dissolving hydrophilic environment. The fast release of Cm-p1–PVA from the nanofibers can be triggered by an extremely high surface area and porosity of the scaffolds. However, some studies suggest crosslinking PVA, aiming to decrease the PVA hydrophilicity and then increase the dissolution time of the PVA fibers.[34,39,40] The synthetic AMP fluorescein labelled inverse-Crabrolin (iCR-fluor) was incorporated into electrospun poly(ε-caprolactone) and exhibited a 30% release rate in the first 30 min. After 2 h, the release of the encapsulated molecule was 50%.[25] The cumulative release of plantaricin 423 from electrospun blends of poly(D,L-lactide) and poly(ethylene oxide) was evaluated by Heunis and colleagues[26] and exhibited a high initial burst release and a more continuous release of bacteriocin over an 8-day period.

Antifungal activity

The activity of the antifungal Cm-p1–PVA loaded nanofibers against *C. albicans* was evaluated by a radial diffusion assay (RDA) by comparing the inhibition halo between 30 mg mL^{-1} amphotericin B, free Cm-p1 and the PVA and Cm-p–PVA fiber mats. The Cm-p1 concentrations were evaluated by HPLC from the release quantification over 24 h and then used for the bioassay. A quantitative list of antifungal activities of the different loading agents and the ratio inhibition measurements is presented in Table 1. In a previous assay, no halo was visualized when the fibers were added directly to a Sabouraud dextrose plate (data not shown). Only 10% Cm-p1–PVA nanofibers were able to inhibit *C. albicans* growth after the nanofibers had been solubilized in distilled water. Despite the Cm-p1 activity, previous results[11] presented higher activity than 10% Cm-p1–PVA nanofibers. According to Hassounah and co-workers,[41] the establishment of hydrogen bonds between the amino groups of the drugs and the alcohol groups of PVA can lead to deactivation of the drugs due to the high polarity of the alcoholic oxygen atom in PVA.[41] In a preceding theoretical structural analysis,[11] it was predicted that Cm-p1 consists of a hydrophilic molecule scoring an impressive average of hydropathicity and displays a minor central hydrophobic region bordered by basic amino acids at the extremes.[11] A three-dimensional theoretical model of Cm-p1 revealed an α-helix conformation with a distribution of net charge caused by exposed cationic histidine (His8) and arginine (Arg2 and Arg10) residues. Leucine (Leu5) and valine (Val7), the hydrophobic preserved region, seem to perform a critical role in the peptide's antifungal activity, favoring peptide-membrane interaction.[11] Furthermore, the amino acid residue, Val7, can be significant in fungal interaction. Studies demonstrated that the pleurocidin lethal effects against *Candida albicans* and other fungi occurs due to the presence of an amidated valine residue at the C-terminus.[42] This same effect was also visualized with the antimicrobial peptide, adenoregulin, against filamentous fungi and Gram-positive and negative bacteria.[43]

Table 1 Quantitative list of nanofiber scaffolds with respect to concentration and halo inhibition in Sabouraud dextrose agar measurements against *C. albicans* ATCC 10231[a]

Compound	Concentration (mg mL^{-1})	Ratio inhibition measurement (mm)[44]
Amphotericin B	30.00	14.10
Free Cm-p1	4.00	9.27
PVA fiber	N/A	N/D
2.5% Cm-p1– PVA fiber	1.92	N/D
5% Cm-p1– PVA fiber	3.04	N/D
10% Cm-p1– PVA fiber	5.26	3.94

[a] N/A: not applicable; N/D: not detectable.

Biocompatibility of Cm-p1–PVA fibers with mammalian cells

HUVEC viability (Fig. 4a) was evaluated in the presence of different nanoscaffolds (the same peptide/polymer ratio was used in the bioassay) using a MTS assay. None of the concentrations of the Cm-p1 scaffolds that were tested affected the HUVEC viability when compared with the PVA scaffolds. These results confirmed preliminary studies conducted by López-Abarrategui and colleagues,[11] where similar results were observed using free Cm-p1 against RAW 264.7 murine macrophage-like cells. However, the proliferation of HUVECs was affected in the presence of 10% Cm-p1–PVA scaffolds, as shown in Fig. 4c. Meanwhile, for the PVA fibers, 2.5% Cm-p1–PVA and 5% Cm-p1–PVA peptide concentrations did not induce significantly lower cell attachment and proliferation in primary endothelial cells.

Moreover, we also tried to better explore the mechanism of action of the peptide fiber analyzed here. Since some antimicrobial peptides act by inducing cell death through reactive oxygen species (ROS) production, we evaluated the ROS production by the HUVECs after 24 h (Fig. 4b). This analysis was performed using the same proportions used for the activity assay (2.5%, 5% and 10%). Only the 10% Cm-p1–PVA scaffolds induced the formation of toxic ROS by the HUVECs (Fig. 4b). Similar data has previously been obtained by using PvD, an antifungal defensin peptide from the *Phaseolus vulgaris* seeds

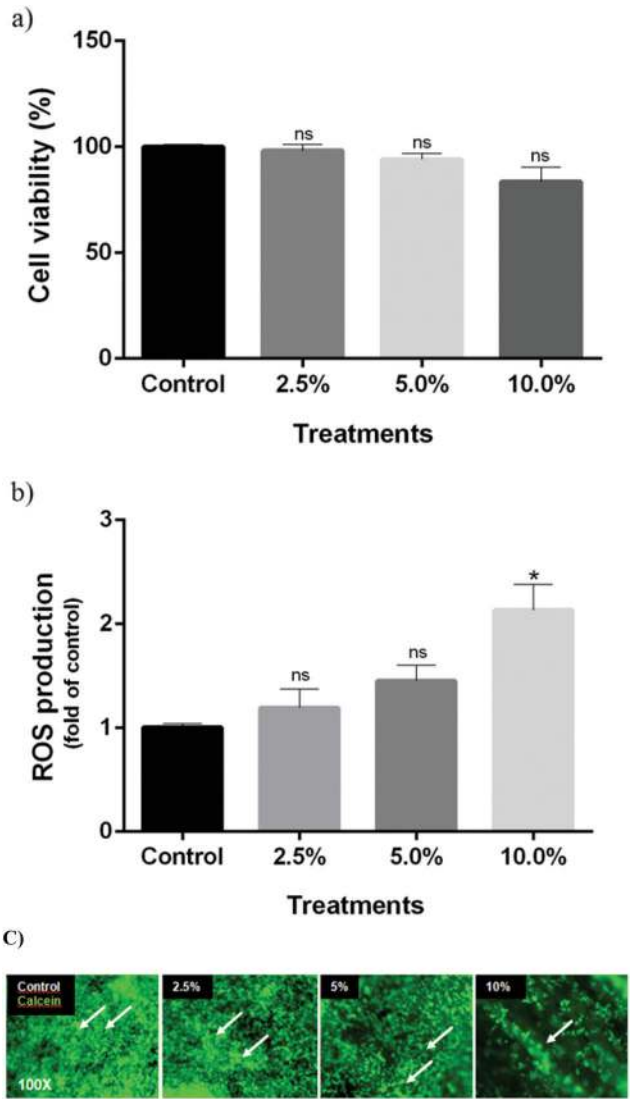

Fig. 4 Biocompatibility of peptide/nanoscaffolds with mammalian cells. Evaluation of (a) HUVEC viability; toxicity profiles of the control scaffold (no peptide) and peptides with different concentrations in the HUVECs. Relative viability was determined by using the MTS assay and all values were normalized to the values obtained with the control group. (b) ROS generation with different scaffold formulations was determined by a ROS assay and represented as fold change compared to the control. (c) Viable HUVECs (in green) in different nanoscaffold groups stained with calcein AM dye, with less cell attachment and proliferation noted in the 10% group (white arrows) compared to the others. The data represent the mean ± SD. NS: no significance. (*$P < 0.1$).

with activity against *C. albicans*. This peptide induces fungal cell death by membrane permeabilization and the stimulation of oxidative stress injury, with the generation of ROS and nitric oxide.[45,46] This same mechanism was also described for another plant defensin, HsAFP1 from *Heuchera sanguinea*,[44] which induces several pro-apoptotic signals including ROS accumulation, leading to cell death. Unlike Cm-p1, both HsAFP1 and PvD were able to induce fungal cell death by ROS generation at low concentrations (5 μg mL^{-1} and 100 μg mL^{-1}, respectively). According to the data in Fig. 4b and bioassay results, it is possible that the Cm-p1 mechanism of action may involve ROS generation due to an improvement in production (Fig. 4b). However, further studies are needed to confirm this hyphothesis.

Furthermore, nanofiber hemolytic activity was evaluated after 24 h of release (ESI, Fig. 3†). No concentrations (2.5%, 5% and 10%) of nanofibers induced hemoglobin leakage. In the same way, in brief experiments, no concentrations of free Cm-p1 were capable of causing hemolysis.[11] Antifungal drugs have several toxicity problems against mammalian cells. The authors of a previous study affirmed that this outcome is probably due to the low hydrophobicity of Cm-p1.[11]

The secretion of pro-inflammatory cytokines, TNF-α (Fig. 5a) and IL-6 (Fig. 5b), from RAW 264.7 macrophages after 24 h of exposure with the control scaffolds (no peptide) and scaffolds carrying different concentrations of Cm-p1 was evaluated. Only the 10% Cm-p1–PVA scaffold presented significant

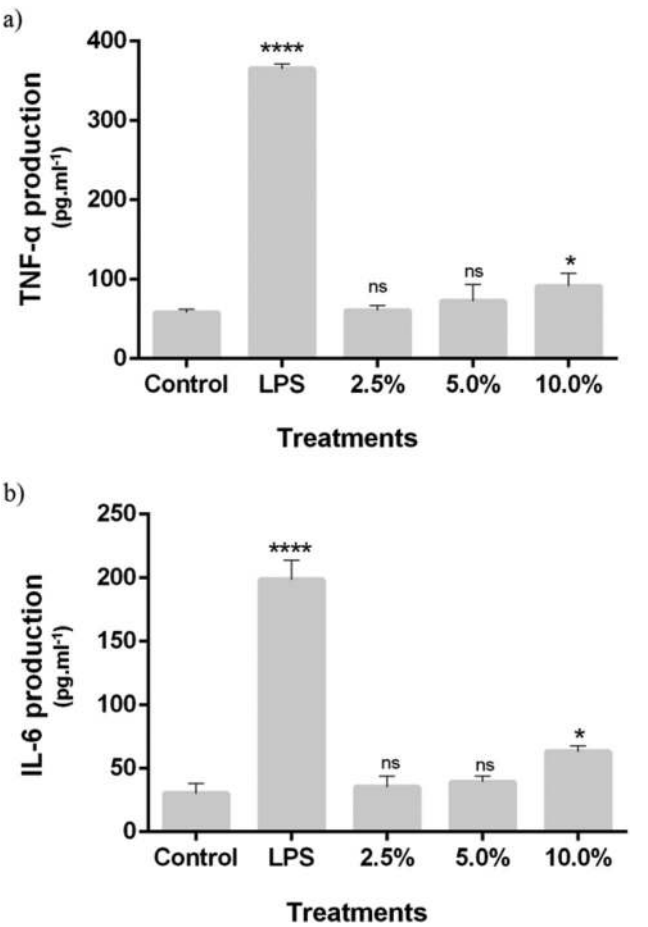

Fig. 5 Evaluation of cytokine pro-inflammatory secretion of TNF-α (a) and IL-6 (b) by RAW 264.7 macrophages, after 24 h of exposure with the control scaffolds (no peptide) and scaffolds carrying different percentages of peptides, as obtained by ELISA analysis. LPS was used as a positive control. The data represent the mean ± SD. NS: no significance. (*$P < 0.1$; ****$P < 0.0001$).

cytokine generation when compared with the control scaffolds. However, this production is 3 and 4 times lower for IL-6 and TNF-α, respectively, in comparison to the LPS-stimulated group. Moreover, the production of proinflammatory cytokines, such as IL-6 and TNF-α, plays an important role, leading to an inflammatory response by inducing other anti-inflammatory mediators, the activation of T cells and the secretion of antibodies by B cells.[47]

In this context, the capacity to induce the secretion of cytokines to promote the recruitment of immune cells of cathelicidins is well known. The release of TNF-α and IL-6 was induced by cathelicidin LL-37 in keratinocytes and immature dendritic cells at much lower concentrations.[48,49] Furthermore, the bacteriocin plataricin A, produced by *Lactobacillus plantarum*, was also shown to increase migration and cell proliferation, as well as stimulating the expression of vascular endothelial growth factor A and IL-8 in keratinocytes.[50] Kindrachuk *et al.*[51] demonstrated that nisin Z presents immunomodulatory activities and modulates the host immune response similarly to natural host defense peptides. Although Cm-p1 slightly induces IL-6 and TNF-α secretion in mammalian cells in higher concentrations, this peptide did not present detectable cytotoxicity. In addition, TNF-α and IL-6 production was seen after 24 h of cell culture incubation, where the peptide release, shown in Fig. 3b, is 5.26 mg mL^{-1}. However, after this period the peptide release decreased greatly, reaching an insignificant value after 72 h of cell culture incubation (Fig. 3b). The cytokine production can be minimized, exposing the cells to nanofibers after 24 h, when the Cm-p1 concentration drops. Nevertheless, it is important to emphasize that Cm-p1 activity will also be minimized. In this way, the induction of low proinflammatory cytokine production happens only in the early period of its use, helping the microorganism's elimination and/or prevention. The low cytokine production favors the opsonization of pathogens, the clearance of apoptotic cells and the activation of complement.[47,52]

Conclusions

In this report we describe the production of nanofibers that encapsulate antifungal peptides. At the moment, few antimicrobial peptides have been incorporated into nanofibers[53] and the use of the electrospinning tool should be explored through the incorporation of antimicrobial peptides. In summary, 10% Cm-p1–PVA concentration was able to decrease the growth of *C. albicans*. Moreover, with this same concentration, Cm-p1 slightly induced ROS generation without affecting the cell viability, as well as being capable of causing low induction of IL-6 and TNF-α production by mammalian cells. Electrospun fibers generated here may be useful as wound care and drug delivery systems. The emerging field of intelligent nanomaterials for medical applications has gained attention in recent decades. However, preclinical development is still a bottleneck to be solved for these advances to reach clinical applications.

Experimental

Materials

Polyvinyl alcohol (PVA) with a hydrolysis degree of 89% and a molecular mass of 134 ± 4 kDa was obtained from Vetec, Brazil. The *Candida albicans* ATCC 10231 strain was obtained from the Universidade Católica Collection and was grown on liquid RPMI medium (Sigma-Aldrich, USA). Mouse RAW 264.7 macrophage cells were purchased from the ATCC (TIB-71) and cultured in DMEM medium supplemented with 10% FBS and 1% penicillin/streptomycin at 37 °C in 5% CO_2. Lipopolysaccharide (LPS) was obtained from InvivoGen. HUVECs (primary human umbilical vein endothelial cells, Lonza) were cultured in endothelial basal medium 2 (EGM-2 BulletKit, Lonza) supplemented with growth factors (hFGF-β, hydrocortisone, VEGF, R3-IGF-1, ascorbic acid, heparin, FBS, hEGF).

Peptide synthesis and purity degree evaluation

The peptide was purchased from enterprise Peptide 2.0 Incorporated,[8] which synthesized the peptide with 95% purity. The Cm-p1 molecular mass was confirmed by using MALDI-TOF MS/MS analysis (Autoflex, Bruker Daltonics, Billerica, MA). The purified peptide was solubilized in a minimum water volume and blended with an α-cyano-4-hydroxycinnamic acid saturated matrix solution (1 : 3, v : v), spotted onto a MALDI TOF target plate and air-dried at room temperature for 10 min. The α-cyano-4-hydroxycinnamic acid matrix solution was made at 50 mM in H_2O–ACN–TFA (50 : 50 : 0.3, v : v : v). The peptide monoisotopic mass was gained in the reflector mode with external calibration, using the Peptide Calibration Standard II (up to 4000 Da mass range, Bruker Daltonics, Billerica, MA). The synthetic peptide concentrations were obtained by using the measurements of absorbance at 205, 215 and 225 nm, as defined by Murphy and Kies (1960).

Electrospun non-woven mats of PVA/peptide

Different concentrations of Cm-p1 (2.5%, 5% and 10%, w/v) were solubilized in 0.5 ml of deionized water and stirred overnight at 70° C. After 12 h, 50 mg of PVA were slowly added in order to produce a 10% w/v solution and stirred at 70 °C until complete solubility was achieved. The electrospinning process was carried out on a horizontal configuration; a 1 mL plastic syringe with a stainless steel capillary (BD, gauge 12) was loaded with the PVA/polypeptide solution and processed at 15 kV supplied by a high voltage source (homemade), with a flow of 0.2 mL h^{-1} using a syringe pump (NE-2000, New Era, Pump Systems Inc.) and a working distance of 10 cm from the needle tip to the collector. The produced mats were collected on aluminum foils.

Scanning electron microscopy

For morphological analysis of the nanofibers by scanning electron microscopy (SEM), a Zeiss DSM 962 (Carl Zeiss, Germany) microscope was used. The nanofiber samples of the cover slip were affixed to the surface of stubs, using double-sided

adhesive conductive carbon tape. Stubs were covered with an ultra-thin gold layer (20 nm) using the Sputter Coat Emitech K550. SEM images were analyzed and captured, and the diameters of the fibers in the mats were determined using 10 000× magnification by the Image J Tool for Windows version 3.0. Statistical analysis was performed using Microsoft Excel's one-way analysis of variance (ANOVA).

Atomic force microscopy measurements

Atomic force microscopy (AFM) images were obtained on a JPK Instruments NanoWizard II (Berlin, Germany) mounted on a Carl Zeiss Axiovert 200 inverted microscope (Jena, Germany). Images were performed in an intermittent contact mode (air) using ACL silicon cantilevers from AppNano (Huntingdon, UK) with a tip radius of 6 nm, a resonant frequency of approximately 190 kHz and spring constant of 58 N m^{-1}. All images were obtained with similar AFM parameter (setpoint, scan rate and gain) values. The scan rate was set between 0.3 and 0.6 Hz and the setpoint was close to 0.3 V. Height and error signals were collected and images were analyzed with the JPK image processing software v. 4.2.53 (JPK Instruments).

Cm-p1–PVA nanofiber release analyses

The Cm-p1–PVA release characterization was made using an *in vitro* elution method.[21] Samples with an area of 2 cm × 2 cm, cut from the electrospun membranes, were put into glass test tubes (one sample per test tube, total number = 3) with 1 mL of phosphate-buffered solution (0.15 mol L^{-1}, pH 7.4) in each. The glass test tubes were kept at 37 °C for 24 h, after which the eluent was removed and evaluated. Fresh phosphate-buffered solution (1 mL) was added for the following 24 h period, and the procedure was sustained for 15 days. Drug concentrations in the eluents were analyzed using the standard curve carried out in RP-HPLC. At the same time, samples with the same area cut from the nanofibers were put into glass test tubes (one sample per test tube, total number = 3) with 1 mL of phosphate-buffered solution (0.15 mol L^{-1}, pH 7.4) in each. The glass test tubes were kept at 37 °C for 0.5, 1, 1.5, 2, 4, 8, 12 and 24 h, after which the eluent was collected and determined by the standard HPLC assay curve. For peptide quantification, a standard curve was carried out with several amounts (0.2, 0.4, 0.6, 0.8 and 1.0 mg) of peptide weighed in an analytical balance (AND GH-202, USA). The standard deviation for the sample weighed was 5% for each application into the C18 analytical column in a linear gradient of 5 to 95% of acetonitrile in 0.01% of trifluoroacetic acid (TFA). The line equation observed, $y = 1297x + 201$ with R^2 value of 0.996, was used to quantify the samples in all the steps of the release measurements.

Antifungal bioassays

A bioassay against fungi was performed by measuring fungal growth inhibition using a radial diffusion assay (RDA).[25] Sabouraud dextrose plates were made by dissolving 10 g L^{-1} peptone, 20 g L^{-1} dextrose, and 4% agar in distilled water, after which the solution was autoclaved. The test solutions were prepared from samples with an area of 2 cm × 2 cm, cut from the electrospun membranes, put into glass test tubes containing 1 mL of autoclaved distilled water and then kept for 24 h at 37 °C and 200 rpm. The samples were then lyophilized and solubilized with autoclaved distilled water. When the plates had hardened, circular holes were made in the medium with the large end of a 2–200 μL pipette tip. Into these holes, 20 μL of the solutions to be tested were added. 10 mL of Sabouraud dextrose medium containing 2 % of agarose was then mixed with a suspension of 5 mL of fungi grown overnight, after which it was poured into petri dishes yielding a thickness of approximately 2 mm. The plates were then set to incubate at 37 °C. Amphotericin B (30 μg ml^{-1}) was used as the positive control. The following day, the plates were inspected for antimicrobial activity against the fungal strain. The activity was recognized as a clear zone of inhibition around the hole, and the larger the diameter of this ring, the higher the activity of the loading agent against this strain, as analysed by the Image J Tool for Windows version 3.0. Statistical analysis was performed using Microsoft Excel's one-way analysis of variance (ANOVA).

Nanoscaffold/peptide immune toxicity analysis toward mammalian cells

Plasma treated nanoscaffold surfaces with different nanofiber formulations (0.3 cm^2) were inserted into each well of a 96-well plate. Plasma surface chemical treatment using a plasma reactor was done to improve the surface hydrophilicity and cell adhesion properties of the polymeric nanoscaffolds. The peptide/polymer ratios used in these experiments were 2.5%, 5% and 10%, the same ratios observed in the antimicrobial analysis. Plasma treatment was used to improve the hydrophilicity of nanoscaffold surface. This procedure was followed by addition of RAW 264.7 macrophages with 2×10^3 cells per well, which were grown for 24 h. As positive control, RAW cells were treated with 100 ng mL^{-1} of LPS. ELISA assays (SA Biosciences) of the conditioned media from different groups were carried out according to the manufacturer's protocol to quantify the secreted cytokines IL-6 and TNF-α by the RAW cells. Each experiment was performed in triplicate.[54–56]

Cell viability assays

In a similar way, cell viability of the HUVECs in the presence of different nanoscaffolds was measured using a Cell Titer 96 Aqueous Non-Radioactive Cell Proliferation MTS Assay (Promega) according to the manufacturer's protocol. To maintain the same standardization, the same peptide/polymer ratios (2.5%, 5% and 10%) were used in this assay. For this, 2×10^4 HUVECs were grown on the different nanoscaffold groups and the absorbance was measured using a plate reader at 490 nm after 24 h of cell culture. Each experiment was performed in triplicate.[57]

Superoxide production analyses

Intracellular production of superoxide by the HUVECs, due to exposure to the peptide/nanoscaffolds, was evaluated using an

intracellular ROS assay (Cell Biolabs, Inc) according to the manufacturer's instructions. Similar to the above-mentioned experimental method, 2×10^4 HUVECs were grown on the nanoscaffolds for 24 h and the fluorescence signals in each well were quantified with a fluorometric plate reader at 480 nm/530 nm. The assay used a cell-permeable fluorogenic probe, 2′,7′-dichlorodihydrofluorescein diacetate, to trace the ROS. The fluorescence intensity in each well is directly proportional to the ROS level within the cell cytosol.[58] In a separate experiment, the cells grown on the scaffolds for 48 h were stained with cell-permeant calcein AM dye (Life Technologies) to trace viability.

Hemolytic activity

The hemolytic activity was determined according to Bignami (1993)[59] and Tramer (2012)[60] with modifications. Earlier, 1 mL of fresh blood from BALB/c mice was fractionated by centrifugation and the red blood cells were recovered in 1% (v/v) PBS. The suspension was washed three times with PBS and aliquoted in microtubes and in PVA and 2.5%, 5% and 10% Cm-p1–PVA; after 24 h of release, the nanofibers were added and set aside for 1 h. Saline solution and 0.1% Triton X-100 were used as the negative and positive control, respectively. After 1 h, the microtubes were centrifuged (1000 *g*; 2 min) and the supernatant was applied in the 96 well plate. The absorbance was measured using a reader at 406 nm (Bio-Tek PowerWave HT, EUA).

Acknowledgements

This work was supported by CAPES, FUNDECT, CNPq, FAPDF, UCB, Fundação para a Ciência e Tecnologia – Ministério da Educação e Ciência (FCT-MEC, Portugal) and the Calouste Gulbenkian Foundation (Portugal).

Notes and references

1 S. Taweechaisupapong, T. Choopan, S. Singhara, S. Chatrchaiwiwatana and S. Wongkham, *J. Ethnopharmacol.*, 2005, **96**(1–2), 221–226.
2 A. C. Costa, C. A. Pereira, J. C. Junqueira and A. O. Jorge, *Virulence*, 2013, **4**(5), 391–399.
3 P. Sudbery, N. Gow and J. Berman, *Trends Microbiol.*, 2004, **12**(7), 317–324.
4 N. A. Gow and B. Hube, *Curr. Opin. Microbiol.*, 2012, **15**(4), 406–412.
5 D. K. Benjamin, Jr., M. L. Hudak, S. Duara, D. A. Randolph, M. Bidegain, G. T. Mundakel, G. Natarajan, D. J. Burchfield, R. D. White, K. E. Shattuck, N. Neu, C. M. Bendel, M. R. Kim, N. N. Finer, D. L. Stewart, A. C. Arrieta, K. C. Wade, D. A. Kaufman, P. Manzoni, K. O. Prather, D. Testoni, K. Y. Berezny, P. B. Smith and T. Fluconazole Prophylaxis Study, *JAMA, J. Am. Med. Assoc.*, 2014, **311**(17), 1742–1749.
6 C. Formosa, M. Schiavone, H. Martin-Yken, J. M. Francois, R. E. Duval and E. Dague, *Antimicrob. Agents Chemother.*, 2013, **57**(8), 3498–3506.
7 J. Otte and S. Vordenbäumen, *Polymers*, 2011, **3**(4), 2010–2017.
8 E. S. Cândido, M. H. S. Cardoso, D. A. Sousa, J. F. C. Viana, N. G. Oliveira-Júnior, V. Miranda and O. C. Franco, *Peptides*, 2014, **55**, 65–78.
9 P. Mendez-Samperio, *Advanced Biomedical Research*, 2013, **2**, 50.
10 C. Lopez-Abarrategui, A. Alba, L. A. Lima, S. Maria-Neto, I. M. Vasconcelos, J. T. Oliveira, S. C. Dias, A. J. Otero-Gonzalez and O. L. Franco, *Curr. Microbiol.*, 2012, **64**(5), 501–505.
11 C. López-Abarrategui, A. Alba, O. N. Silva, O. Reyes-Acosta, I. M. Vasconcelos, J. T. Oliveira, L. Migliolo, M. P. Costa, C. R. Costa, M. R. Silva, H. E. Garay, S. C. Dias, O. L. Franco and A. J. Otero-Gonzalez, *Biochimie*, 2012, **94**(4), 968–974.
12 Z. Zou, T. Liu, J. Li, P. Li, Q. Ding, G. Peng, Q. Zheng, X. Zeng, Y. Wu and X. Guo, *J. Biomed. Mater. Res., Part A*, 2014, **102**(5), 1286–1293.
13 S. M. Mandal, A. Roy, D. Mahata, L. Migliolo, D. O. Nolasco and O. L. Franco, *J. Antibiot.*, 2014, **67**, 771–775.
14 L. Chronopoulou, S. Sennato, F. Bordi, D. Giannella, A. D. Nitto, A. Barbetta, M. Dentini, A. R. Togna, G. I. Togna, S. Moschini and C. Palocci, *Soft Matter*, 2014, **10**(12), 1944–1952.
15 P. Zahedi, I. Rezaeian, S. Ranaei-Siadat, S. Jafari and P. Supaphol, *Polym. Adv. Technol.*, 2010 (21), 77–95.
16 J. Bao, B. Yang, Y. Sun, Y. Zu and Y. Deng, *J. Biomed. Nanotechnol.*, 2013, **9**(7), 1173–1180.
17 A. M. Abdelgawad, S. M. Hudson and O. J. Rojas, *Carbohydr. Polym.*, 2014, **100**, 166–178.
18 A. A. Dongargaonkar, G. L. Bowlin and H. Yang, *Biomacromolecules*, 2013, **14**(11), 4038–4045.
19 R. Lalani and L. Liu, *Biomacromolecules*, 2012, **13**(6), 1853–1863.
20 L. Chenwen, F. Ruoqiu, Y. Caiping, L. Zhuoheng, G. Haiyan, H. Daqiang, Z. Dehua and L. Laichun, *Int. J. Nanomed.*, 2013 (8), 4131–4145.
21 D. W. Chen, Y. H. Hsu, J. Y. Liao, S. J. Liu, J. K. Chen and S. W. Ueng, *Int. J. Pharm.*, 2012, **430**(1–2), 335–341.
22 D. W. Chen, J. Y. Liao, S. J. Liu and E. C. Chan, *Int. J. Nanomedicine*, 2012, **7**, 763–771.
23 R. Dave, P. Jayaraj, P. K. Ajikumar, H. Joshi, T. Mathews and V. P. Venugopalan, *J. Biomater. Sci., Polym. Ed.*, 2013, **24**(11), 1305–1319.
24 T. T. Ruckh, R. A. Oldinski, D. A. Carroll, K. Mikhova, J. D. Bryers and K. C. Popat, *J. Mater. Sci.: Mater. Med.*, 2012, **23**(6), 1411–1420.
25 T. H. Eriksen, E. Skovsen and P. Fojan, *J. Biomed. Nanotechnol.*, 2013, **9**(3), 492–498.
26 T. Heunis, O. Bshena, B. Klumperman and L. Dicks, *Int. J. Mol. Sci.*, 2011, **12**(4), 2158–2173.
27 T. D. Heunis, C. Smith and L. M. Dicks, *Antimicrob. Agents Chemother.*, 2013, **57**(8), 3928–3935.

28 H. B. Lindner, A. Zhang, J. Eldridge, M. Demcheva, P. Tsichlis, A. Seth, J. Vournakis and R. C. Muise-Helmericks, *PLoS One*, 2011, **6**(4), e18996.
29 H. Sarig, S. Rotem, L. Ziserman, D. Danino and A. Mor, *Antimicrob. Agents Chemother.*, 2008, **52**(12), 4308–4314.
30 N. I. Torres, K. S. Noll, S. Xu, J. Li, Q. Huang, P. J. Sinko, M. B. Wachsman and M. L. Chikindas, *Probiotics and Antimicrobial Proteins*, 2013, **5**(1), 26–35.
31 R. Sridhar, S. Sundarrajan, J. R. Venugopal, R. Ravichandran and S. Ramakrishna, *J. Biomater. Sci., Polym. Ed.*, 2013, **24**(4), 365–385.
32 Y. Jia, J. Gong, X. Gu, H. Kim, J. Dongd and X. Shen, *Carbohydr. Polym.*, 2007, **67**(3), 403–409.
33 M. S. Peresin, Y. Habibi, A. H. Vesterinen, O. J. Rojas, J. J. Pawlak and J. V. Seppälä, *Biomacromolecules*, 2010, **11**(9), 2471–2477.
34 Y. Liu, B. Bolger, P. A. Cahill and G. B. McGuinness, *Mater. Lett.*, 2009, **63**, 419–421.
35 E. Yang, X. Qin and S. Wang, *Mater. Lett.*, 2008, **62**, 3555–3557.
36 S. Agarwal, J. H. Wendorff and A. Greiner, *Polymer*, 2008, **49**, 5603–5621.
37 A. J. Meinel, O. Germershaus, T. Luhmann, H. P. Merkle and L. Meinel, *Eur. J. Pharm. Biopharm.*, 2012, **81**(1), 1–13.
38 L. L. Zhang, L. H. Huang, Z. X. Zhang, D. J. Hao and B. R. He, *Chin. Med. J. (Engl.)*, 2013, **126**(20), 3891–3896.
39 J. Zeng, H. Hou, J. H. Wendorff and A. Greiner, *Macromol. Rapid Commun.*, 2005, **26**, 1557–1562.
40 J. M. Gohil, A. Bhattacharya and P. Ray, *J. Polym. Res.*, 2006, **13**, 161–169.
41 I. A. Hassounah, N. A. Shehata, G. C. Kimsawatde, A. G. Hudson, N. Sriranganathan, E. G. Joseph and R. L. Mahajan, *J. Biomed. Mater. Res. A*, 2013, **102**, 4009–4016.
42 J. Lee and D. G. Lee, *J. Microbiol. Biotechnol.*, 2010, **20**(8), 1192–1195.
43 W. Cao, Y. Zhou, Y. Ma, Q. Luo and D. Wei, *Protein Expression Purif.*, 2005, **40**, 404–410.
44 A. M. Aerts, L. Bammens, G. Govaert, D. Carmona-Gutierrez, F. Madeo, B. P. Cammue and K. Thevissen, *Front. Microbiol.*, 2011, **2**, 47.
45 F. Guilhelmelli, N. Vilela, P. Albuquerque, L. D. Derengowski, I. Silva-Pereira and C. M. Kyaw, *Front. Microbiol.*, 2013, **4**, 353.
46 E. O. Mello, S. F. F. Ribeiro, A. O. Carvalho, I. S. Santos, M. d. Cunha, C. Santa-Catarina and V. M. Gomes, *Curr. Microbiol.*, 2011, **62**, 1209–1217.
47 J. R. Machado, D. F. Soave, M. V. d. Silva, L. B. d. Menezes, R. M. Etchebehere, M. L. Monteiro, M. A. D. Reis, R. R. Corrêa and M. R. Celes, *Mediators Inflammation*, 2014, **2014**, 1–10.
48 M. Afshar and R. L. Gallo, *Veterinary Dermatology*, 2013, **24**(1), 32–38.
49 A. J. Duplantier and M. L. V. Hoek, *Front. Immunol.*, 2013, **4**, 143.
50 D. Pinto, B. Marzani, F. Minervini, M. Calasso, G. Giuliani, M. Gobbetti and M. D. Angelis, *Peptides*, 2011, **32**(9), 1815–1824.
51 J. Kindrachuk, H. Jenssen, M. Elliott, A. Nijnik, L. Magrangeas-Janot, M. Pasupuleti, L. Thorson, S. Ma, D. M. Easton, M. Bains, B. Finlay, E. J. Breukink, H. Georg-Sahl and R. E. Hancock, *Innate Immun.*, 2013, **19**(3), 315–327.
52 P. W. Dempsey, S. A. Vaidya and G. Cheng, *Cell. Mol. Life Sci.*, 2003, **60**, 2604–2621.
53 A. Brandelli, *Mini-Rev. Med. Chem.*, 2012, **12**(8), 731–741.
54 Q. Cheng, B. L. Lee, K. Komvopoulos, Z. Yan and S. Li, *Tissue Eng., Part A*, 2013, **19**(9–10), 1188–1198.
55 A. Hasan, A. Memic, N. Annabi, M. Hossain, A. Paul, M. R. Dokmeci, F. Dehghani and A. Khademhosseini, *Acta Biomater.*, 2014, **10**(1), 11–25.
56 S. Prakash, A. Khan and A. Paul, *Expert Opin. Biol. Ther.*, 2010, **10**(12), 1649–1661.
57 A. Paul, C. B. Elias, D. Shum-Tim and S. Prakash, *Sci. Rep.*, 2013, **3**, 2366.
58 J. Koontz and A. Kontrogianni-Konstantopoulos, *J. Biol. Chem.*, 2014, **289**(6), 3468–3477.
59 G. S. Bignami, *Toxicon*, 1993, **31**, 817–820.
60 F. Tramer, T. D. Ros and S. Passamonti, *Methods Mol. Biol.*, 2012, **926**, 203–217.